

上海交通大学

SHANGHAI JIAO TONG UNIVERSITY

学士学位论文

BACHELOR'S THESIS



论文题目：基于机器学习的多模态磁共振脑影像计算分析
及其精神分裂症诊断中的应用

学生姓名：庄惠翔

学生学号：5140309131

专 业：测控技术与仪器

指导教师：刘满华

学院（系）：电子信息与电气工程学院仪器系

基于机器学习的多模态磁共振脑影像计算分析及其精神分裂症诊断中的应用

摘要

精神分裂症是影响全球 2100 多万人的重要脑疾病之一。多模态磁共振影像为检测精神分裂症引起的脑解剖结构和功能的病理变化和临床诊断提供了重要的依据。在本毕业设计中,我们研究了基于机器学习的多模态磁共振图像计算和分析算法,旨在对精神分裂症进行自动诊断并识别具有区分度的生物标志物。首先,我们分别对结构性和功能性脑磁共振影像进行图像处理以提取代表结构和功能信息的特征。其次,我们提出了结合稀疏编码和多核线性支持向量机的分类模型对首发精神分裂症和健康对照组进行特征识别与分类。再次,由于临床评分能提供更准确的精神分裂症评估,本文提出了稀疏编码和基于相似矩阵的随机森林相结合的回归模型,用于识别与评分最相关的生物标志物和预测精神分裂症的临床评分。稀疏编码从每种模态的影像特征中选择一组相关的特征,而随机森林用于结合多模态特征进行回归并且根据特征在评分预测中的重要性进行排序。最后,对上述方法进行了实验验证。对于分类模型,我们对上海精神卫生中心招募的首发精神分裂症患者和健康对照组进行了模型测试。实验结果表明我们提出的结合稀疏编码和多核线性支持向量机方法对首发精神分裂症与健康对照的分类准确率达到 84.29%, ROC 曲线下面积为 81.64%。对于临床评分估计,我们为提出的结合稀疏编码和随机森林回归模型进行了基于多中心的多模态影像数据试验,结果表明相关系数达到 0.51 ± 0.10 。对于选择的有区分度的生物标志物进一步分析显示:小脑一皮层的功能连接对首发精神分裂症鉴别诊断的贡献最大;白质中的内侧丘系、内囊;以及属于边缘系统、默认模式网络、运动系统和额叶的灰质皮层可以帮助评估精神分裂症的严重程度。实验结果表明本文所提出的机器学习方法可以从多模态磁共振影像中提取有用的信息并识别重要的生物标志物以改善精神分裂症的诊断。

关键词: 精神分裂症诊断, 多模态磁共振成像, 稀疏编码, 支持向量机, 随机森林, 生物标志物识别

MACHINE LEARNING BASED MULTIMODAL MAGNETIC RESONANCE IMAGING ANALYSIS FOR SCHIZOPHRENIA DIAGNOSIS

ABSTRACT

Schizophrenia (SZ) is one of the important brain diseases affecting more than 21 million people in the world. Multimodal magnetic resonance (MR) images provide the important biomarkers to detect the pathological changes in both brain function and anatomy for diagnosis of SZ. In this thesis, we have developed the multimodal MR image computing and analysis algorithms based on machine learning methods, aiming to automatically diagnose SZ and identify the discriminative biomarkers. First, the structural and functional MR brain images have been processed to extract the anatomical and functional features for the representation. Second, we have proposed a combination model of sparse coding (SC) and multi-kernel linear support vector machine (SC+MKL-SVM) to perform the classification between first-episode schizophrenia (FES) and healthy controls and identify the discriminative features. Third, since the clinical scores provide more accurate evaluation of SZ, we have proposed a regression model by combination of the SC and proximity-based random forest (SC+RF) for predicting clinical scores and identifying the most correlated biomarkers of SZ. SC has been applied as an initial selection of a group of related features from each feature type, while random forest (RF) has been applied to combine multimodal features for regression as well as to sort the importance of features in score prediction. For classification, our proposed algorithms have been tested on the subjects of FES and healthy controls recruited from the Shanghai Mental Health Center.

Experimental results show that our proposed SC+MKL-SVM method has achieved the classification accuracy of 84.29% and the area under the curve (AUC) of 81.64% for discriminating SZ from healthy controls. For score estimation, we have conducted a multicenter trial based on our proposed SC+RF method. The result has achieved the correlation coefficient of 0.51 ± 0.10 . Further analyses of discriminative biomarkers have shown that cerebellar-cortical functional connectivity (FC) contributes most to the FES diagnosis; white matter measures in medial lemniscus, internal capsule, and cortical measures belonging to limbic cortex, default mode network (DMN), motor cortex, and frontal lobe can help estimate the severity of SZ. The results have verified that the proposed methods can extract useful information from multimodal MR images and identify important biomarkers to improve the diagnosis of SZ.

Key words: Schizophrenia diagnosis, Multimodal Magnetic Resonance Imaging (MRI), Sparse coding, Support Vector Machine, Random forest, Biomarker identification

Contents

Chapter 1 Introduction	1
1.1 Schizophrenia and Clinical Assessment	1
1.2 Magnetic Resonance Imaging (MRI)	2
1.3 Machine Learning Based SZ Diagnosis	3
1.4 Our Contributions	4
Chapter 2 Materials & Feature Extraction	5
2.1 Participants	5
2.2 Data Acquisition	6
2.3 MRI Preprocessing and Feature Extraction	7
2.3.1 Structural MRI	7
2.3.2 DTI	8
2.3.3 Resting-state fMRI	8
2.3.4 Normalization	9
Chapter 3 Multimodal Classification for FES Diagnosis	11
3.1 Overview	11
3.2 Feature Selection Based on Sparse Coding	12
3.3 Multimodal Combination Based on MKL-SVM	13
3.4 Experimental Results	14
3.4.1 Single-modal Classification	15
3.4.2 Multimodal Classification	16
3.4.3 Biomarker Identification	18
3.5 Chapter Summary	22
Chapter 4 Multimodal Regression for Clinical Score Prediction	23
4.1 Overview	23
4.2 Random Forest	23
4.3 Multimodal Combination Based on RF	25
4.4 Experimental Results	26
4.4.1 Multimodal Regression	26
4.4.2 Biomarker Identification	28
4.5 Chapter Summary	32
Chapter 5 Conclusion	33
REFERENCE	34
APPENDIX	38
ACKNOWLEDGEMENTS	44
PUBLICATIONS	45

Chapter 1 Introduction

Machine learning, relying on data analytics and the computational ability of computer [1], has widely replaced or assisted many pieces of complex artificial works in various fields. Psychosis, as well as dementia, have received greater attentions in modern life. Not only for researchers and psychiatrists, more and more people have realized the harm of such mental diseases. Thus, it is increasing demand to improve the psychosis and dementia diagnosis. Besides the traditional artificial diagnosis by clinical score assessment, in the field of neuroscience, psychiatrists explore the pathology and brain changes in the patients using some medical imaging techniques, such as magnetic resonance imaging (MRI), positron emission tomography (PET), and electroencephalogram (EEG), etc.. Each imaging has different modalities, such as structural MRI, functional MRI for MRI, and FDG-PET, Amyloid PET for PET. Many specific features can be extracted from different modalities to provide an extensive vision of the intricate cerebral lesions for psychiatrists. Meanwhile, this brings about large computations and more complicated image processing. Machine learning is a promising method which can be applied to solve these hot issues in the field of medical imaging. For mental disease detection and diagnosis, machine learning researches on medical imaging has made a great contribution and has been regarded as a powerful aid. Classification and regression problems can be solved by machine learning models, to automatically differentiate the patients from the healthy people, to explore the relationship with clinical assessment, and to find out biomarkers related to the symptoms.

1.1 Schizophrenia and Clinical Assessment

Schizophrenia (SZ) is one of the important brain diseases which affects about 21 million people globally, and the rate of lifetime mortality suffered from SZ is up to 13% [2]. Neuropsychology and clinical research indicate that the symptoms of SZ mainly

include cognitive dysmetria, altered perception, auditory hallucination, motor retardation, etc. The 4th edition of *Diagnostic and Statistical Manual of Mental Disorders* (DSM-IV) stated that, as in the case with many medical terms, schizophrenia "lacks a consistent operational definition that covers all situations" [3]. Clinical score assessment is a widely-accepted method to directly evaluate the severity of syndromes. The prevailing clinical score of SZ is the Positive and Negative Syndrome Scale (PANSS). Kay firstly provided the standard explanation of PANSS score in 1989 [4]. The PANSS score contains 30 sub-scores corresponding to several syndromes of SZ. The total score can be generally separated into 3 parts: positive, negative, general syndrome score. The positive and negative syndrome scores both have 7 items, and the general syndrome score has 16 items. For each sub-score, the value represents the degree of severity from 1 to 7 in increasing order. In clinical, SZ will be diagnosed by clinical scores, and future antipsychotic therapy will be conducted for disease control. The utilized medicines may include typical antipsychotic agents like haloperidol, a major tranquilizer, and atypical ones, such as clozapine, risperidone, olanzapine, sertindole et al, according to the cardinal symptoms of the specific schizophrenia.

1.2 Magnetic Resonance Imaging (MRI)

Besides clinical score, medical imaging is another powerful tool for the diagnosis of psychosis. It has been found in clinic that distinct types of symptoms are related to different morphological changes and functional disconnections in brains. MRI, an imaging technique which detects magnetic resonance (MR) information, can provide powerful imaging modalities to detect the brain changes relate to the disease and make discrimination between the healthy persons and the disorders. For the brain structure, grey matter (GM) anatomy can be clearly observed on T1-weighted images— the technique of structural MRI (sMRI). White matter (WM) connection and the track of fibers can be detected by diffusion tensor imaging (DTI). Blood oxygen level dependent (BOLD)-functional MRI (fMRI), which helps detect the temporal-related signal of the blood oxygen fluctuations [5], can reveal the functional work in the brain

according to the state of the patient being scanned: task-based or resting state (rs). From rs-fMRI, we can have a clear view on the regional functional connections in the brain. These techniques all greatly contribute to the diagnosis of dementia and psychosis.

Brain changes have been proved to be combined with the SZ and the clinical event feedbacks. Rajji [6] concluded that functional abilities have a great impact on the stage of schizophrenia according to several longitudinal studies, and functional changes were also detected in hippocampus-related regions [7]. The studies in [7-11] all mentioned the relationship between antipsychotic (medication) and the changes of brain volume as a whole or in certain regions, such as left hippocampus and lateral ventricle. According to these previous studies, we found the feasibility of analyzing MR data for tracking the progression of psychosis.

1.3 Machine Learning Based SZ Diagnosis

With the development of MR imaging technologies, especially the multimodal MR imaging, there are a huge amount of data captured from MR images, which make it difficult for manual image analysis. Mass data from the multiple modalities require computational methods to make better use of these data and achieve high efficiency and accuracy of diagnosis. Thus, machine learning methods have been widely investigated for multimodal brain MR image analysis, with the advantages to deal with high-dimensional features and automatically identify the features most related to the pathology of psychosis. According to different tasks, the machine learning modeling can be divided into two categories: classification and regression. For classification, there are many classifiers proposed for disease diagnosis, such as the most popular support vector machine (SVM) classifier and random forest classifier [12]. For regression, the Least Square-SVM (LS-SVM) method is often applied to predict the longitudinal clinical scores and model the SZ progression [13-15]. Because of its efficiency to deal with the small sample data, SVM is still widely used in medical imaging field for both classification and regression. Multi-kernel SVM also can be used to combine the features from multiple modalities [16]. Recently, other machine learning

methods have been proposed to handle with high-dimensional features of medical images for the computer aided disease diagnosis [12, 17-20]. It is still challenging to combine the features from multiple modalities and achieve high performance for SZ diagnosis using multimodal MR images.

1.4 Our Contributions

In this thesis, we have investigated the machine learning technologies to analyze the multimodal MR data including sMRI, DTI, and rs-fMRI, for schizophrenia diagnosis. We have developed 2 machine learning models for both classification and regression tasks. First, we have proposed to apply sparse coding (SC) based on multi-variable analysis to select the most discriminant features from each modality. Then, for classification, the multi-kernel SVM has been applied to combine multimodal features and classify drug-naïve first-episode schizophrenia (FES) patients and the healthy persons. For regression, random forest (RF) has been used to develop a multimodal regression model for clinical score prediction and identifying the predictive biomarkers. Our study has the following contributions: 1) we have extracted and successfully combined the features containing both structural and functional information from the multiple modalities of MRI; 2) we have developed machine learning methods to identify the informative biomarkers, classify the drug-naïve FES from healthy controls and predict the clinical scores; 3) We have conducted multi-center experiments on SZ clinical score prediction to evaluate the proposed methods. The result has revealed the universality of the selected biomarkers predictive to the disease.

The rest of this thesis is organized as follows. Chapter 2 presents the materials and the participants used in this study, and the detailed introduction of the image preprocessing and feature extraction steps. Chapter 3, 4 introduce the proposed multimodal classification and regression models, respectively and present the experimental results and analysis. Chapter 5 concludes our thesis.

Chapter 2 Materials & Feature Extraction

2.1 Participants

There are 2 sets of participants with 3 modalities of MR images prepared for different tasks in our study. Set I consists of multimodal MR brain images captured from single center. Table 2.1 shows demographic statistics and clinical analysis of the participants in Set I. The participants are from 2 groups: FES group consisting of 40 patients with first-episode schizophrenia (with no medicine intake record for the disease) recruited from Shanghai Mental Health Center, China (SMHC) and the healthy control (HC) group consisting of 32 normal subjects (female/male=16/16, age= 27.16 ± 4.28 , range: 20~39 years) from local community. For subject cleaning, 1 HC participant was eliminated due to lack of scanning data (HC017). Furthermore, we removed 2 subjects (HC003, HC010) after inspecting their living conditions (HC003 was in lactation during scanning time, and HC010 worked as a sailor, who lived a long time in a special environment). Finally, 29 HCs are participated in our study. There are 5 SZ patients (SZ004, SZ015, SZ022, SZ023, SZ043) without clinical scores in FES group. Since missing clinical scores had no effect on the classification result, they are used for classification but are excluded for regression. All SZ patients met criteria of schizophreniform disorder in Diagnostic and Statistical Manual of Mental Disorders, 5th Edition (DSM-V). The psychopathology and symptom severity were assessed using PANSS.

Set II includes multimodal MR brain images captured from 3 centers. Table 2.2 shows demographic statistics and clinical analysis of the participants in Set II. The 176 SZ participants met criteria of schizophreniform disorder in DSM-V. 35 FES subjects are same as those in Set I from SMHC with clinical scores, 70 SZ subjects from COBRE study [21, 22], and 71 SZ subjects from BrainGluSchi study in the

Schizconnect database (<http://www.schizconnect.org/>) [23]. All the SZ patients in this set have the PANSS clinical scores.

Table 2.1 Demographic statistics and clinical analysis of the participants in Set I

Group	Drug-naïve FES	Healthy Controls
Number of subjects	40 (*35)	29
Age (years)	26.88±5.81	27.03±4.32
Gender (females/males)	18/22	15/14
Education (years)	12.87±3.41	14.21±2.37
PANSS total score	72.62±17.10	
Course of psychosis (month)	6.51±11.61	

35 of 40 FES patients have clinical scores. The statistics are presented in the form of mean ± standard deviation.

Table 2.2 Demographic statistics and clinical analysis of the participants in Set II

Center	SMHC	COBRE	BrainGluSchi
Number of subjects	35	70	71
Age (years)	27.13±5.90	38.36±13.76	35.68±13.93
Gender (females/males)	17/18	15/55	8/69
PANSS total score	73.54±17.47	60.17±15.59	63.00±20.27

The statistics are presented in the form of mean ± standard deviation.

2.2 Data Acquisition

In set I, all sMRI and rs-fMRI data were collected on a 3.0-T Siemens Verio MR Scanner (Siemens AG, Erlangen, Germany) with a 32-channel head coil at SMHC. During the scanning process, all the participants were required to lay supinely with inflatable pillows placed between the head and coil to minimize movement artifacts. The participants were instructed to rest quietly with their eyes closed but to remain awake and avoid systematic thinking during scanning. The main parameters of imaging were as follows: anatomical T1-weighted images were acquired using a magnetic preparation fast gradient echo (MPRAGE) sequence with echo time (TE)=3.65ms, repetition time (TR)=2530ms, field of view (FOV)=256mm, slice thickness=1.0mm, and slice number=224. DTI data were acquired along the AC/PC line, throughout the whole brain, TE=90ms, TR=10200ms, FOV=256mm, slice thickness=2.0mm. Blood

oxygen level dependent (BOLD) images with TE=30ms, TR=2000ms, FOV=220mm, slice thickness=4.0mm, voxel size=3.4×3.4×4.0mm, matrix size=256×256, and slice number=180. COBRE and BrainGluSchi MR image data in set II were also collected on a 3.0-T Siemens Verio MR Scanner (Siemens AG, Erlangen, Germany) at the center of the Mind Research Network (MRN). The detailed scan information is available in the **Attachment 1, 2**.

2.3 MRI Preprocessing and Feature Extraction

2.3.1 Structural MRI

For sMRI data, Freesurfer 6.0.0 [24, 25] is used for the preprocessing, as well as the feature extraction. This software provides a completely automated pipeline of cortical and subcortical nuclei segmentation and surface reconstruction process. ‘recon-all’ is a batch program and is the core command of the software. It has 3 auto-reconstruction sections and totally 31 steps during a complete procedure, and all the subjects need to go through the whole steps automatically to get the ultimate detailed statistics. The first section contains motion correction and conform, non-uniform (NU) intensity normalization, Talairach registration, intensity normalization, skull stripping to get the basic preparation for segmentation and calculation. In the next two sections, subcortical segmentation is initially done and the statistics of segmented subcortical structures are recorded. Sequentially, white matter is segmented and surface is generated for both hemispheres. Parcellation can be based on 3 different atlases (the Killiany/ Desikan parcellation atlas, Destrieux atlas, DKT atlas). In the stats table, we have access to 9 measures for each segment based on different registration protocols. The statistical measures such as standard deviations derived from some of the other measures are excluded. Altogether, we choose 6 kinds of measures in our study [26]. They are: 1) cortical thickness (th); 2) gray matter volume (vol); 3) surface area (area), which is calculated by computing the area of every triangle after tessellation; 4) mean curvature (meancurv), computed by using the registration surface based on the folding patterns; 5) curvature indices (curvind); 6) folding index (foldind). To detect the potential errors

in segmentation and achieve more accurate results, manual interventions need to conduct for each subject using GUI tools in Freesurfer when the fully automated 31 processing steps were finished. White matter segmentation errors may high-frequently happen among No.130 to No.170 coronal plane slides. The old segmentation files should be replaced by the manual-edited ones and the following steps where these old files were first generated in the pipeline are rerun.

When the processing is finished, the statistical outputs of the cortical parcellation are recorded, and the information of proposal measures on each labeled region for each subject can be extracted from these output files. As to the 6 cortical measures, we can get different numbers of features due to different kinds of atlas. Finally, we choose the stats based on Destrieux atlas consisting of 74 ROIs in each hemisphere. In all, the total feature number of sMRI can be expressed as follows:

$$6 \times 74 \text{ ROIS} \times 2 \text{ Hemisphere} = 888 \text{ features} \quad (2-1)$$

2.3.2 DTI

DTI data is processed by FMRIB Software Library (FSL) [27] and Pipeline for Analyzing brain Diffusion imAges (PANDA). The raw diffusion weighted images (DWIs) are firstly processed by motion and eddy current correction, then brain extraction (Here we set a threshold of 0.25), finally calculation of fractional anisotropy (FA), mean diffusivity (MD). These steps are completed in FSL. After obtaining FA and MD images, we utilize PANDA 1.3.1 to normalize every subjects' FA and MD images to standard MNI152 template, smoothed images with a Gaussian kernel of 2mm, and calculate DTI parameters of 50 ROIs in whole brain, which are labeled in JHU-Atlas. We select $50 \times 2 = 100$ features (50 FA, 50 MD) for further classification.

2.3.3 Resting-state fMRI

Rs-fMRI imaging data preprocessing is conducted with SPM8 package, rest1.8 and DPARSF2.3 advanced edition, under Matlab 2013a (Mathworks, USA). The first 10 time points of 180 time points should be removed for subjects' adaption to the environment and the stabilization of the machine. The time series of slices are

uniformed to 15th slice (slice scanned in the middle). Realignment is conducted to reduce head motion artifacts using DPARSF 2.3. Subsequently, all corrected functional data are normalized to EPI templates. After this, smoothing is also performed to raise SNR and the effect of normalization. Detrend is conducted to correct the linear drifting of signal. Temporal waveform of each voxel is band-passed into 0.1-0.8HZ to reduce the effect of low frequency drift and high signal noise. Fractional amplitude of low-frequency fluctuation (fALFF) is calculated in the following based on voxels. The total number of voxels is $63 \times 71 \times 63 = 281799$. Voxels located out of the brain have 0 value and are deleted. 70831 voxels with fALFF value are eventually selected as the features.

Functional connectivity (FC) matrix is constructed by employing an automatically labeled template (i.e., automated anatomical labeling (AAL) to parcellate the brain into 116 regions of interest). The representative time series of each ROI is obtained by averaging the time series of each voxel within that region. A Fisher's-Z transformation is further applied to the correlation matrices to improve the normality of the correlation coefficients. One value of FC revealed the connection between 2 different ROIs. So, 116 ROIs can generate $116 \times 115 \div 2 = 6670$ FC values.

Suppose the subject number is N , and the number of features is Q . For each feature matrix, its size can be represented as $N \times Q$. For sMRI and DTI, considering the dimension of features in each modality is relatively small, we combine different types of measurements together and generate one matrix for each modality. As to rs-fMRI, which has 2 kinds of features with large dimension: FC (6670 features) and fALFF (70831 features), creating 2 matrices for this modality is suitable. Finally, we gain 4 feature matrices from 3 modalities. The dimensions are: 888 for sMRI, 100 for DTI, 6670 for FC (rs-fMRI), 70831 for fALFF (rs-fMRI). These 4 feature matrices will be served as the original input of the following classification and regression models.

2.3.4 Normalization

Since the multimodal features containing different information have different ranges, normalization is usually required to make all features in a specific range. Normalization

can reduce the effect of unit diversity of the extracted measurements and make the multimodal features comparable. Generally, there are two methods widely used for normalization [28]. One is Min-Max scaling to a fixed range. The other method is z-score normalization. In this method, the features are scaled to have the same average sum-of-squares and they are normalized into a same distribution. In this work, the Min-Max scaling method is used for all multimodal features to ensure each feature to be scaled to a fixed range of 0 to 1 across all the subjects.

Chapter 3 Multimodal Classification for FES Diagnosis

3.1 Overview

In this chapter, we have proposed a multimodal classification algorithm by combining the multimodal MR images for FES diagnosis. Fig.3.1 shows the flowchart of the proposed algorithm. First, the multimodal features are extracted as described in Chapter 2. Then, sparse coding (SC) is applied to select the most discriminant features based on multi-variable analysis for each modality. Finally, multi-kernel linear SVM (MKL-SVM) is applied to combine the multimodal features for the final classification.

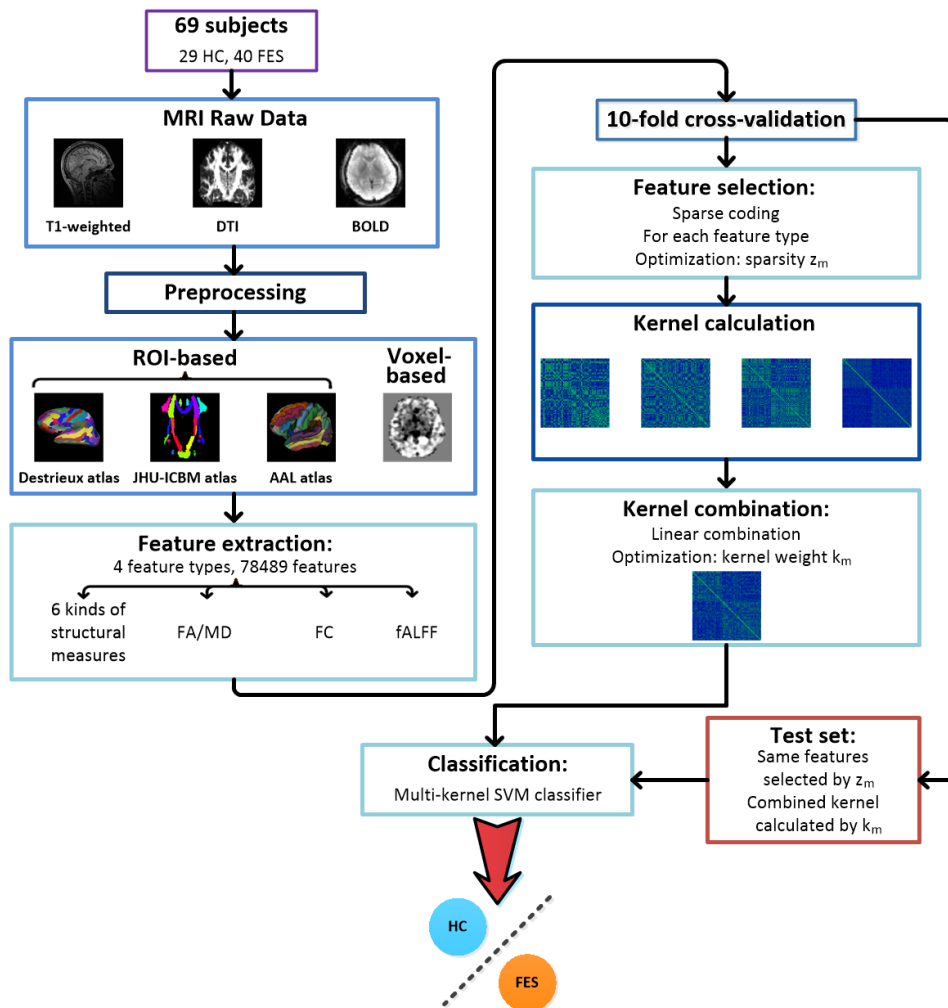


FIGURE 3.1 The flowchart of the proposed multimodal classification algorithm

3.2 Feature Selection Based on Sparse Coding

To avoid missing the important features for classification, we have extracted the features as many as possible from multimodal MR images. Thus, the total extracted multimodal features have huge dimensionality (>70000), when compared with the small number of subjects. It is necessary to identify the discriminative features to facilitate disease classification and interpretation. Traditionally, the t-test method is often used to find significant biomarkers by individually evaluating the discrimination of each feature with p-value. However, this method has completely ignored the correlations of imaging features and failed to consider the discrimination of multiple variable combination. This is not suitable for our application because the informative imaging biomarkers may be distributed over more than one brain regions. Thus, to identify the informative imaging biomarkers, a multivariate model is learned to consider the combinations of features over the distant brain regions for handling the multivariate interactions in feature selection. Sparse coding as a machine learning method has been widely applied to the task of feature selection [29, 30], as well as classification [31, 32] in the field of face recognition. In this work, a sparse coding method with $L1$ -regularization [33, 34] has been applied to select the informative features for each modality [31]. Unlike the traditional two-sample t-test, SC considers the combination of multi-variable features to achieve a global significance.

Let \mathbf{A} represent a $N \times Q$ feature matrix. The p th row of \mathbf{A} is the feature vector of the image from the p th participant. \mathbf{y} denotes the class labels of all participants with the p th element being the class label of the p th participant. Thus, a linear regression model can be used to generate the class outputs with a set of features as follows:

$$\mathbf{y} = \mathbf{A}\vec{\omega} + \varepsilon \quad (3-1)$$

where $\vec{\omega} = (\omega_1, \omega_2, \dots, \omega_N)$ be a vector of coefficients assigned to the corresponding features, and ε is an independent error term. The class output can be characterized as the linear combination of features. One popular method to solve this problem is the

least square optimization. When the number of features is large, sparsity is imposed on the coefficients to choose a small number of relevant features for classification. The $L1$ -regularized sparse coding can be formulated as:

$$\bar{\omega} = \operatorname{argmin}_{\omega} \|y - \mathbf{A}\bar{\omega}\|_2^2 + z\|\bar{\omega}\|_1, \quad s. t. \bar{\omega}_i \geq 0, \forall i \quad (3-2)$$

where z is the sparsity regularization parameter which controls the amount of zero coefficients of $\bar{\omega}$. The non-zero elements in $\bar{\omega}$ indicate that the corresponding features are more relevant to the classification. When the z value increases, the number of non-zero elements in $\bar{\omega}$ decrease, and more features will be selected to be relevant. Thus, the $L1$ -regularized sparse coding method provides an effective multivariate regression model to select a subset of relevant features by taking into consideration both the correlations of features to the class labels and the combinations of individual features [35]. By adjusting the values of sparsity, various numbers of features can be selected without ranking. This method can jointly select the features from multiple contiguous brain regions based on the population difference.

3.3 Multimodal Combination Based on MKL-SVM

To combine the features selected by SC from multiple modalities, one simple method is to concatenate all features into a vector and then design a linear support vector machine (SVM) classifier to make classification. But the concatenated feature vector is of high dimension which will degrade the classification performance. Instead, we apply the MKL-SVM classifier to combine the multimodal features for classification. Different from the conventional linear classifier, the kernel based SVM classifier maps the linearly nonseparable feature space in the original lower-dimensional space to a higher-dimensional feature space, where they are more likely to be separable, with a kernel function. In the higher-dimensional space, a maximum margin hyperplane is calculated with the SVM for classification. Let K be a kernel function, and x_1, x_2 be the feature vectors of 2 subjects. The kernel used for SVM can be denoted as $K(x_1, x_2)$. To combine the multimodal features, we apply the multi-kernel SVM method for

multimodal classification. The kernel matrices for different modalities are combined into a mixed kernel by a linear weighted combination as follows:

$$K(x_1, x_2) = \frac{\sum_{m \in M} k_m K_m(x_1^m, x_2^m)}{\sum_{m \in M} k_m} \quad (3-3)$$

where $M = \{\text{sMRI, DTI, FC, fALFF}\}$ is a set of features in different types, and $k_m \in [0,1]$ represents the weight assigned to feature type m . Based on the mixed kernel, the traditional SVM such as LIBSVM can be used for classification. In our implementation, LIBSVM toolbox [36] has been used to implement the SVM classifier and the linear kernel with a default value for the parameter C (i.e., $C = 1$) has been used for single/multi-modal classification tests.

3.4 Experimental Results

In this section, we will present the experimental results of the multimodal MRI analysis for diagnosis of FES and give some discussions. The 3 MRI modalities, i.e., sMRI, DTI and rs-fMRI from set I are used in our experiments. The classifier is implemented with LIBSVM 3.22 toolbox [36] in Matlab 2014b for classification. For each type of feature, sparse coding method has been implemented for feature selection using the SLEP package downloaded at <http://www.public.asu.edu/~jye02/Software/SLEP>. The details on the materials used in the experiments have been introduced in Chapter 2. To statistically evaluate the classification performance, the standard 10-fold cross-validation has been performed in the experiments. Each time, 1 fold of data set is used for test, while the remaining 9 folds are used for training. In the experiments, the parameters to be optimized are sparsity z , which can be adjusted to change the number of selected features, and the weights k_m . Grid search from 0 to 1 at step of 0.05 for z and from 0 to 1 at step of 0.1 for k_m are used to optimize these parameters.

To evaluate the classification results, classification accuracy, sensitivity and specificity are calculated as follows:

$$\text{accuracy} = \frac{\text{TN} + \text{TP}}{\text{TN} + \text{FP} + \text{FN} + \text{TP}} \% \quad (3-4)$$

$$\text{sensitivity} = \frac{\text{TP}}{\text{FN} + \text{TP}} \% \quad (3-5)$$

$$\text{specificity} = \frac{\text{TN}}{\text{TN} + \text{FP}} \% \quad (3-6)$$

where TP is the number of FES patients which are correctly classified, TN is the number of HC correctly classified, FP denotes the number of HCs falsely classified, and FN is the number of falsely classified FES. Thus, the sensitivity denotes the accuracy to classify the real patients while the specificity evaluates the accuracy to classify the healthy controls. In addition, ROC curve has been demonstrated by sensitivity and 1-specificity at different thresholds and area under the curve (AUC) has been calculated to evaluate the classification performance. In the following subsections, we will present the classification results of single/multi-modality and discuss the selected biomarkers.

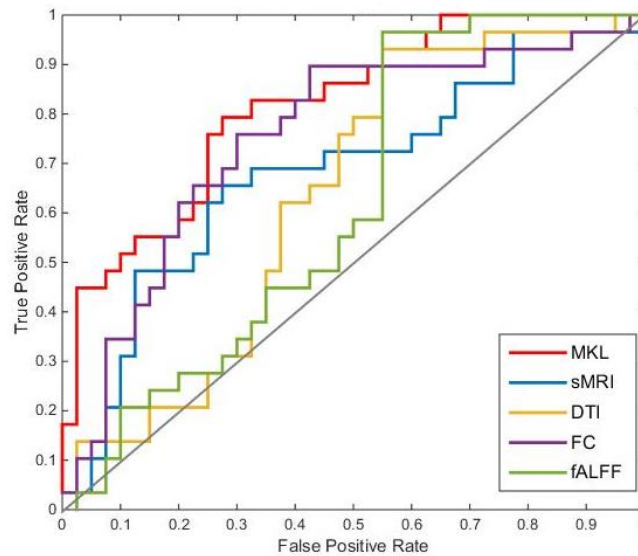
3.4.1 Single-modal Classification

The first experiment is to test the classification with single modality. There are 4 types of features (denoted as sMRI, DTI, FC, fALFF) extracted from 3 MRI modalities: sMRI, DTI, fMRI. Table 3.1 shows the classification accuracies and the feature numbers for single modality of sMRI, DTI, FC, fALFF as well as the multimodal classification. The comparison of their corresponding ROC curves are demonstrated in Fig.3.2. From these results, we can see that FC feature of rs-fMRI can achieve the best single-modal classification result with 75.24% of accuracy and 75.26% of AUC, when compared with those of other features. The fALFF and DTI features have relatively low discriminative ability. In addition, these results also show that the multimodal classification with 84.29% accuracy performs better than any single modalities, showing the effectiveness of our proposed method. Comparing the numbers of original and selected features, we can see that SC can effectively identify the informative features to improve the classification performance. Subjects can be correctly classified with less than 5% features selected by SC, which indicates that a large number of MRI features are redundant for classification.

Table 3.1 Classification results of first-episode schizophrenia patients and healthy controls using single-modal and multi-modal features.

Feature	Accuracy (%)	Sensitivity (%)	Specificity (%)	AUC (%)	# of features	# of selected features
sMRI	71.19	77.50	63.33	68.19	888	4
DTI	67.86	72.50	61.67	63.45	100	9
FC	75.24	80.00	68.33	75.26	6670	39
fALFF	69.29	80.00	55.00	61.90	70831	1662
Multimodal	84.29	92.50	73.33	81.64	78489	1714

AUC: area under the curve; #: the feature dimension.



MKL: the multimodal classification by multi-kernel linear SVM. The grey diagonal line denotes random classification result.

FIGURE 3.2 ROC curves of linear SVM classifiers

3.4.2 Multimodal Classification

After feature selection by SC, we have calculated the linear kernel matrices representing the 4 types of features and MKL-SVM classifier has been applied for

multimodal classification. The results have also been recorded in Table 3.1 and Fig.3.2. The performance is better than any single ones with 84.29% accuracy and 81.64% AUC, showing that combination of multiple modalities by our proposed method has significantly improved the classification results. Moreover, Table 3.2 and 3.3 have shown the results of classification accuracy and AUC, respectively, with different combinations of multiple MRI modalities. The experiments are performed by gradually adding a new type of features. First, we test the classification performances of each single modality shown in the first row of Table 3.2, 3.3. Second, we combine the sMRI with the features of other types, i.e., DTI, FC and fALFF. The results are shown in the second row of Table 3.2, 3.3. From these results, we can see that the classification performances have been improved (accuracy from 71.19% to 74.29%, 75.71% and 74.05%; AUC from 68.19% to 68.97%, 75.52% and 68.45%) by combing sMRI with other feature types. Third, the features of FC and fALFF are added to the sMRI+DTI combination and the classification performances are further improved as shown in the third row of Table 3.2, 3.3 (accuracy from 74.29% to 78.57% and 75.48%; AUC from 68.97% to 79.31% and 73.02%). Finally, fALFF features are added to the sMRI+DTI+FC combination, and the classification performance has finally been improved to the best (accuracy from 78.57% to 84.29%; AUC from 79.31% to 81.64%). The results indicate that adding any kind of features to the previous combination can improve the performance. The combination of all multimodal features achieves the best classification performance for disease diagnosis.

Table 3.2 The comparison of accuracy in different combinations

Step\Combined:	sMRI (%)	DTI (%)	FC (%)	fALFF (%)
1:-	71.19	67.86	75.24	69.29
2:sMRI	-	74.29	75.71	74.05
3:sMRI+DTI	-	-	78.57	75.48
4:sMRI+DTI+FC	-	-	-	84.29

Table 3.3 The comparison of AUC in different combinations

Step\Combined:	sMRI (%)	DTI (%)	FC (%)	fALFF (%)
1:-	68.19	63.45	75.26	61.90
2:sMRI	-	68.97	75.52	68.45
3:sMRI+DTI	-	-	79.31	73.02
4:sMRI+DTI+FC	-	-	-	81.64

3.4.3 Biomarker Identification

This subsection aims to analyze the discriminant features selected from the 3 MRI modalities for disease interpretation. We have examined the selected multimodal features by SC with the optimal regularization parameter for single-modal classification. In our experiments, the standard 10-fold CV has been used. The selected features are different for different folds due to the different training data. Thus, we compute the frequency of feature selected in 10 folds. We have identified the imaging features with the frequency larger than a threshold (set to 5 in our experiments) as the biomarkers. The identified biomarkers for the multimodal features in sMRI and DTI have been listed in **Appendix I**. Fig.3.3-3.6 illustrate these biomarkers separately. We have referred to the corresponding papers of these atlas to determine the region indices and names [37-39].

For sMRI (recorded in Fig.3.3 and **Appendix I**), the identified biomarkers are the cortical thickness in the left superior segment of the circular sulcus of the insula (No. 49), the mean curvature of left planum temporale or temporal plane of the superior temporal gyrus (STG) (No.36), the curvature index of left posterior transverse collateral sulcus (No.51), and right long insular gyrus and central sulcus of the insula (No.17).

For DTI based on JHU-ICBM atlas (recorded in Fig.3.4 and **Appendix I**), among the 100 features (50 ROIs for FA & MD), region number 1 to 50 represent FA features and 51 to 100 represent the MD features. The FA changes in left superior corona radiata

(No.26), left fornix (cres) / stria terminalis (No.40), left posterior thalamic radiation (include optic radiation) (No.30); MD changes in right uncinate fasciculus (UF) (No.47), right superior cerebellar peduncle (No.13), right posterior thalamic radiation (include optic radiation) (No.29), right cingulum (cingulate gyrus) (No.35). Right cingulum (hippocampus) (No.37) identified as the significant biomarkers in both FA and MD variance.

For the FC results based on AAL template, each feature represents a functional connection between 2 regions parcellated by AAL atlas. From Fig.3.5, we find the most discriminant FCs concentrate in: sub-regions in cerebellar lobe with intrinsic connections, and those to the cortical regions; left temporal pole: STG to thalamus and cerebellar regions; right parahippocampal gyrus (PHG) to left calcarine and bilateral lingual gyrus; bilateral postcentral gyrus (PoCG) and paracentral lobe to bilateral thalamus, caudate, and cerebellar regions. Other seed regions, such as orbitofrontal cortex (OFC), right rectus, and basal ganglia, et al.

For fALFF based on $61 \times 73 \times 61$ voxels, each selected feature represents a voxel. Thus, we have mapped the selected voxels to the surface and drawn the mapping representing the voxels' distribution, which has been shown in Fig.3.6. The most related fALFF voxels mainly gather in bilateral occipital lobe, precuneus, and cuneus. Other regions including left angular gyrus (ANG), bilateral lingual gyrus, calcarine, and several cerebellar regions possess small-scale gathering of fALFF voxels.

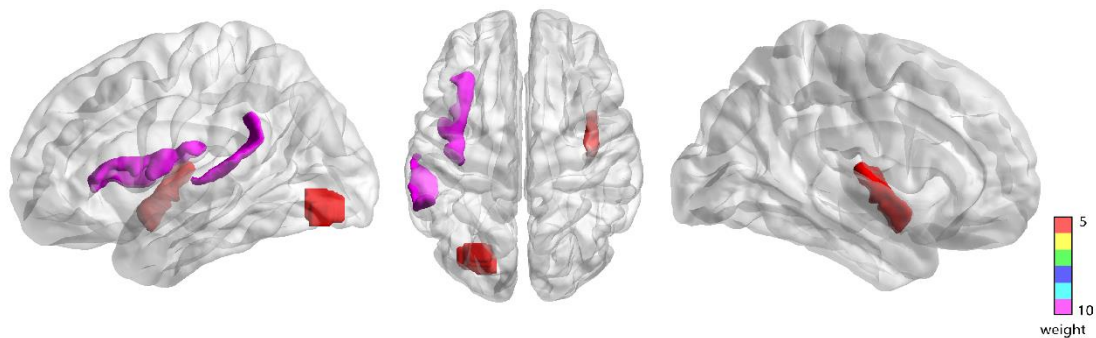


FIGURE 3.3 The significant ROIs of sMRI measures in the surface map

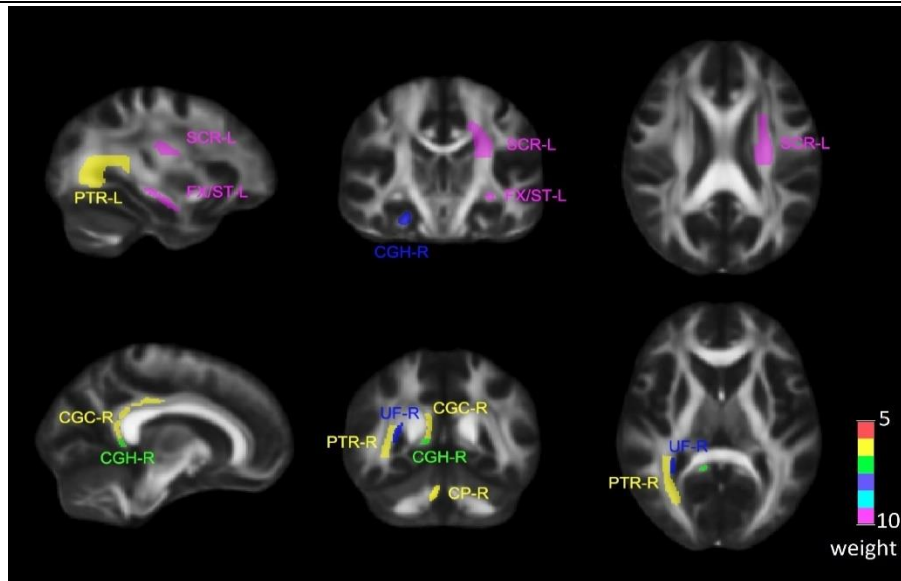
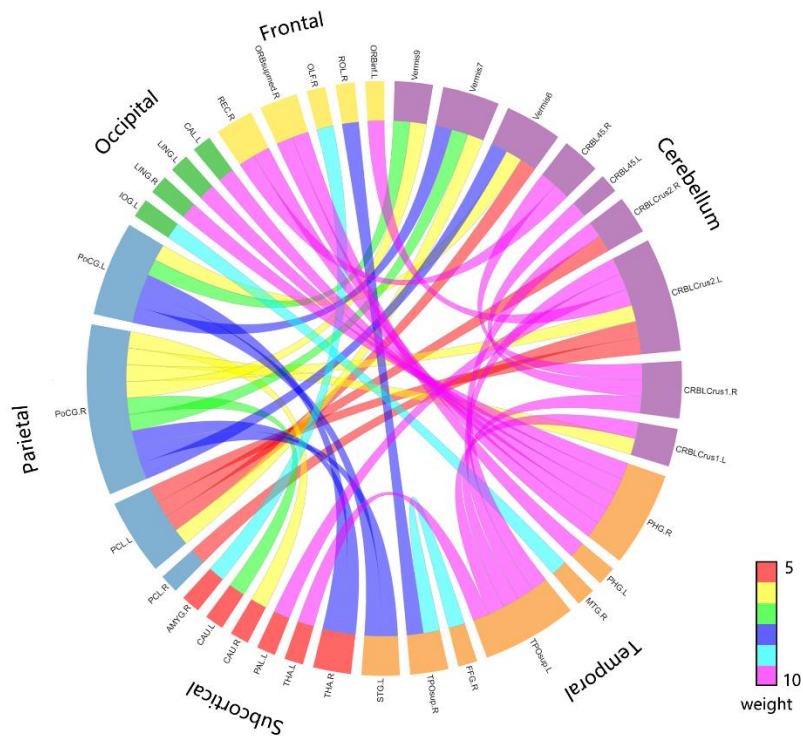


FIGURE 3.4 The significant ROIs of DTI measures



The labels on the circle denote the ROIs in AAL atlas acting as nodes in FCs. The nodes are divided into 6 regions with 6 colors according to [39]. The edges are presented by the bands with different colors that represent the frequency.

FIGURE 3.5 The connection map of top FC features

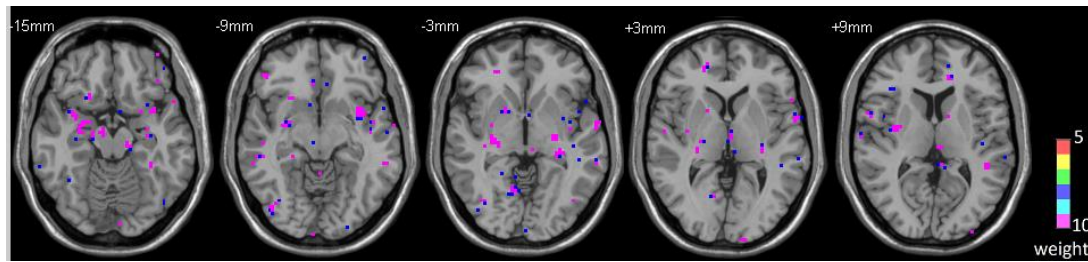


FIGURE 3.6 Map of selected voxels of fALFF in several axial slices

From these results, we can explore the pathology of first-episode schizophrenia. For functional features, according to the results in Table 3.1, FCs contribute most to the diagnosis of drug-naïve FES. Among the discriminative FC pairs, cerebellar regions connected to cortical regions are the most common ones. FCs abnormalities including cerebellum have been widely reported in SZ patients [40-42]. Also, a recent study first reported functional abnormalities in drug-naïve FES patients cerebellum [43]. Moreover, our study has found the selected fALFF voxels also include cerebellar regions. Cerebellum is considered to not only take charge of balance control, but to play a role in conceptual activity and emotion state [44]. The cortical regions with most connections with cerebellum are mainly in left temporal pole and STG, key regions in affective network (AN) [39]. We suppose cerebellum-to-AN connections lead to the emotional abnormality of first-episode schizophrenia. We can also detect some potential pathologies by other functional features. Medial temporal subsystem of DMN (bilateral PHG, precuneus, ANG included), which is one of the most frequently reported networks for drug-naïve FES [45-48], can affect autobiographical memory and future simulations [49]; the sensory-motor network (SMN) [39], mainly bilateral PoCG to subcortical region connections included, can lead to the integration disability of sensory information with motor actions [50]. We suggest that the syndromes caused by these functional network impairments are significantly related to early onset schizophrenia. Compared with FCs, structural measures are not so discriminative to FES. Besides left STG in AN, the only proof of cortical changes happen in limbic system (especially for

insula), which leads to disorders of external sensory integration and interoception [51]. Structural connections are mainly in the anatomy typically work for memory (e.g. UF, fornix, hippocampus). Prefrontal–thalamo–hippocampal circuit, in charge of working memory [52, 53] and goal-directed spatial navigation [54], is also mentioned. These structural connection damages have been widely reported in SZ patients regardless of the course of disease and the patients’ age [55-59]. Considering DTI measures are among the least discriminative features in our study (see Table 3.1), we suppose the symptom of memory impairment is mild in drug-naïve FES.

Referring to the description and categorization of PANSS [4, 60], through overall consideration, emotional discomfort relates to cerebellum, AN; cognitive dysmetria and sensory processing disability relate to DMN, limbic system; motor reaction retardation relates to SMN are the significantly obvious symptoms of drug-naïve first-episode schizophrenia. Working memory and spatial sensing impairment are mild in drug-naïve FES and might get worse in the course of disease.

3.5 Chapter Summary

In this chapter, we have proposed a multimodal classification method by combining the SC and multi-kernel SVM for the auto-detection and early diagnosis of first-episode schizophrenia. In our study, a large number of features are extracted from multi-modality MR images. SC is effective to identify the discriminative features in each modality through multi-variable learning, since the disease-induced abnormal changes often happen in multiple contiguous brain regions, instead of isolated ROIs or voxels. Multi-kernel SVM classifier has been applied to combine the 4 selected multimodal features, which can improve the classification performance for early detection and diagnosis of schizophrenia.

Chapter 4 Multimodal Regression for Clinical Score Prediction

4.1 Overview

In this section, we have proposed a multimodal regression algorithm for PANSS clinical score prediction to achieve more accurate diagnosis of SZ. Fig.4.1 shows the flowchart of the proposed algorithm. Similar to classification, SC is also used for feature selection. The random forest (RF) method is used to compute the proximity measures and make the final multimodal regression. In addition, the classical multidimensional scaling (MDS) is applied to the proximity matrix to generate embedded feature data in a lower dimension, which would serve as the input of the final regression model.

4.2 Random Forest

RF can be an ensemble supervised classifier or predictor of T decision trees in the forest. For regression task, decision trees act as regression trees. As to each regression tree in the forest, the training samples are randomly selected to establish the training set, which is known as bootstrap aggregation (bagging) [61]. Given a set of data with the scale of N , bootstrap sampling will make the pick by N times randomly and with replacement to form a sample bag. In this way, the unpicked data for each tree can be generated, which is called out-of-bag (OOB) dataset. The OOB set is used for self-validation, to decide the growth of the regression tree. The bagging has a similar effect as cross-validation, intrinsically ensures the cogence of statistical evaluation.

Besides bagging, RF has another intrinsic property of feature selection, which is derived from the mode of tree growth [62]. Each node in the tree contains a selected feature to divide the current subset. During the growth of a tree, each node is determined by finding a feature that can minimize the difference of the left-subset predicting error and the right-subset predicting error, which means to best split the current set. When the OOB predicting error is below to a default threshold, the node will stop splitting

and be considered as a terminal node. RF can not only select features, but also give their ranking of the importance by evaluating the OOB predicting error [62].

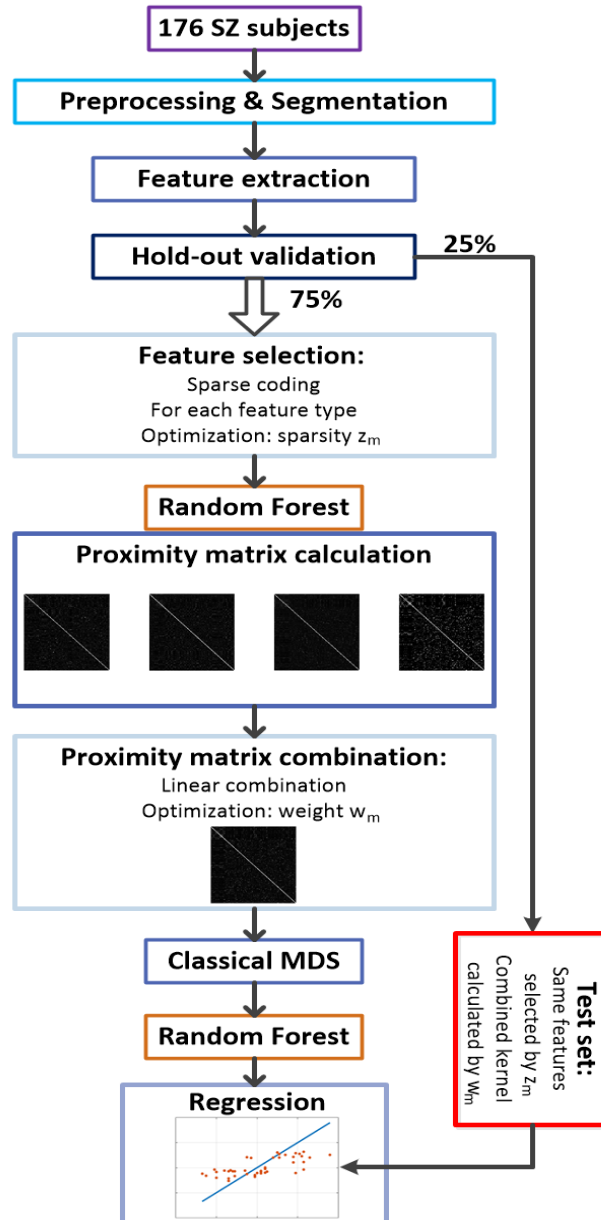


FIGURE 4.1 Flowchart of the proposed multimodal regression algorithm

When a test subject goes through each tree of the forest, it will fall into a terminal node and obtain a predicting score. The final prediction result $P(y)$ is the unweighted average of the predicting scores $p_t(y)$ given by T trees [63]. The formulation is shown as follows:

$$P(y) = \frac{1}{T} \sum_{t=1}^T p_t(y) \quad (4-1)$$

After training, the RF generates proximity measures [64, 65]. Proximity matrix, $\mathbf{P}_{N \times N}$, is calculated when all the input subjects pass down the T trees in the forest. If subject n_i and n_j finish in the same terminal node of a tree, their proximity p_{ij} is increased by 1. The final pairwise proximity measures are normalized by T , i.e., the total number of trees. Since the proximity of a subject to itself is 1, the diagonal elements in \mathbf{P} are always 1. Other elements in the matrix are in $[0,1]$. The proximity matrix can be written as:

$$\mathbf{P} = \begin{pmatrix} 1 & p_{12} & \cdots & p_{1i} \\ p_{21} & 1 & \cdots & p_{2i} \\ \vdots & \vdots & \ddots & \vdots \\ p_{j1} & p_{j2} & \cdots & 1 \end{pmatrix}_{N \times N} \quad (4-2)$$

Proximity matrix preserves the characteristics of the original subjects, i.e. the features, and represents them in a mathematical form. It also serves to depress the features with small importance, since they contribute little to the proximity measures. In fact, proximity matrix plays a similar role as the kernel of SVM, which gives a hint to the feature combination.

4.3 Multimodal Combination Based on RF

After calculating the corresponding proximity matrix for each type of features, the matrices can also be linearly combined into a new proximity matrix to fulfill the multimodal combination as follows:

$$\mathbf{P} = \sum_{m \in M} \alpha_m \mathbf{P}_m \quad (4-3)$$

where $\sum_{m \in M} \alpha_m = 1$, $M = \{\text{sMRI, DTI, FC, fALFF}\}$. However, the proximity matrices always possess redundant proximity information, which may act as a barrier to pursue for a better predicting performance. Thus, dimensionality reduction is considered. Classical MDS is a dimensionality reduction method with the aim of generating manifolds that are optimal for the feature storage in a relatively low dimension. It is

applied on the distance matrix to generate a reduced coordinate embedding for the feature vectors based on eigenvalue calculation. The proximity matrix is transformed into a distance matrix with element $d_{ij} = 1 - p_{ij}$ [66] as follows:

$$\mathbf{D} = \begin{pmatrix} 0 & d_{12} & \cdots & d_{1i} \\ d_{21} & 0 & \cdots & d_{2i} \\ \vdots & \vdots & \ddots & \vdots \\ d_{j1} & d_{j2} & \cdots & 0 \end{pmatrix}_{N \times N} \quad (4-4)$$

The output of MDS contains the matrix of coordinates \mathbf{X} , representing a lower-dimension embedding for the information of distance. Furthermore, a goodness-of-fit parameter G [12] is computed for evaluation:

$$G = \frac{\sum_{i=1}^k \lambda_i}{\sum_{i=1}^N (\lambda_i > 0)} \quad (4-5)$$

where λ is the eigenvalue and k is the number of selected eigenvectors which also represents the dimension of the ultimate manifold space. G is set to 0.9 by experience. The final reduced k -dimensional matrix, possesses the multimodal feature information, can serve as an input of the final RF regression model.

4.4 Experimental Results

In this section, we will present the regression experiments, the results comparison for score estimation, and discuss the predictive biomarkers in detail. The proposed regression algorithm is test on set II with 176 SZ subjects from 3 study centers with PANSS score records.

4.4.1 Multimodal Regression

The algorithm is implemented in Matlab 2014b with the class ‘Treebagger’. According to the bagging property, the hold-out validation has been used to split test set into training and test sets. First, SC has been used for feature selection, and the RF models have been trained based on the 4 feature matrices independently for proximity matrix calculation. Then, RF has been again used for the final prediction. Classical MDS has been added to proximity matrices for dimensionality reduction. When establishing the

RF model, the number of trees in the forest, T , has to be globally determined. The way of setting T is to observe the OOB predicting error, The OOB error figure is helpful for finding the proper number of trees for all the RFs in the experiments, see **Appendix II**. The estimates of the OOB error are consistently stable when $T \gtrsim 300$, for insurance, we have set $T = 1000$ for all the experiments [12]. 2 parameters: sparsity z and weighting factor α_m have been optimized similarly via grid searching through training to achieve the best regression performance.

According to the description of PANSS score in [4, 60] and the score table we have obtained, the total PANSS score can be divided into positive, negative, and general score. The outputs of the regression model are the estimated total, positive, negative, and general PANSS scores.

We have randomly held-out 25% data for testing and 75% for training and have conducted 10 times repeated experiments. To evaluate the predicting performance, the Pearson's correlation coefficient (CORR) and the root mean square error (RMSE) between the actual and estimated PANSS scores have been computed by average. Additionally, the determination coefficient r^2 with the value of the square of CORR, has been used to evaluate the power of regression line in data representation. The multimodal predicting results are shown in Table 4.1.

Table 4.1 Performance of prediction on PANSS scores (mean±std)

Scores	CORR	RMSE	r^2
PANSS-total	0.51±0.10	16.01±3.04	0.27±0.11
PANSS-positive	0.48±0.10	5.09±0.35	0.24±0.10
PANSS-negative	0.47±0.11	5.24±0.72	0.23±0.10
PANSS-general	0.52±0.11	8.94±1.59	0.28±0.10

From Table 4.1, we can see that our proposed regression model has a satisfactory predicting performance on all 3 parts of PANSS scores and the total one. We also find that the CORR results of 4 score tests are similar. PANSS general score prediction has reached the best CORR. It may imply that the general syndrome items in PANSS system

are more correlated with the selected features.

Additionally, we have tested the predicting performance of the single-modal models. We have compared the 4 single-feature-type models with the multimodal model by CORR. The results are shown in Table 4.2. Accordingly, for some parts of PANSS scores, some feature types actually cannot provide any prediction (e.g. DTI for PANSS negative score, FC for PANSS general score). Through multimodal combination, the predicting performance of the regression model has been significantly improved. This improvement has indicated the effectiveness of our proposed method.

Table 4.2 Single-feature-type vs multimodal predicting performance (mean±std)

Feature	PANSS-total	PANSS-positive	PANSS-negative	PANSS-general
sMRI	0.21±0.19	0.20±0.15	0.21±0.19	0.28±0.13
FC	0.17±0.14	0.19±0.12	0.14±0.18	0.05±0.16
fALFF	0.23±0.13	0.20±0.11	0.12±0.10	0.18±0.10
DTI	0.26±0.13	0.18±0.12	0.07±0.17	0.30±0.16
Multimodal	0.51±0.10	0.48±0.10	0.47±0.11	0.52±0.11

4.4.2 Biomarker Identification

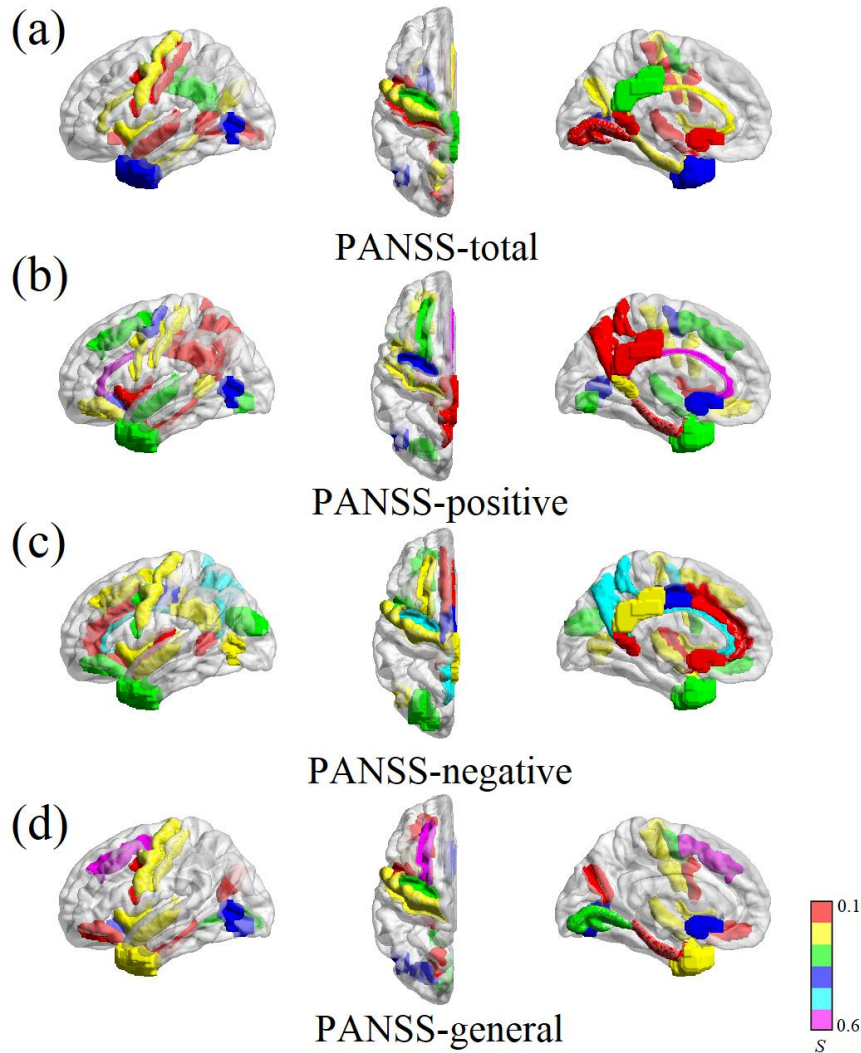
In the regression model, SC serves as an initial feature selection to select a group of discriminative features. RF makes a second feature selection intrinsically and provides the importance of features for ranking. Thus, the proposed regression method can select the top contributive features quantitatively across the modalities. This advantage benefits the identification of predictive biomarkers. During the repeated experiments, the importance values s have been separately aggregated for all participated features, and the final importance values have been judged by the aggregation of importance S , during the 10 times repeat. S could be ranked in global considering the difference in the strategy of feature extraction and scale of feature measurements across the modalities (i.e. the ROI-based sMRI, DTI, FC features and the voxel-based fALFF features). We have discussed the biomarkers within categories under different criterions. We set the threshold of S with 0.1 to the ROI-based features. For sMRI and DTI, the

biomarkers with the $S > 0.1$ for 4 types of clinical scores have been listed in **Appendix III**. The corresponding ROIs have been depicted in Fig.4.2 and Fig.4.3 respectively; Fig.4.4 has presented the topology graphs for FC with nodes containing 6 colors determined by [39] for AAL atlas, and edges containing different thickness representing the values of S . For voxel-based fALFF, considering the scale, we have decided not to apply ranking information. Instead, the selected voxels for 4 types of PANSS scores have been all depicted with 4 colors in Fig.4.5.

Different from the biomarker identification in Section 3.4.3, the subjects for regression are from multiple studies and centers and the biomarkers have been double selected by SC+RF for regression. If we compare the selected predictable biomarkers with the biomarkers selected during classification tasks in Chapter 3, there exists similarities and differences. For similarities, limbic system and DMN have been still among the top brain system containing predictive biomarkers across the modalities, and the abnormality in cerebellar connections with cortical regions has also been highly related to the disease. As for differences, we have found that FCs are no longer the best feature types, and anatomical measures seem to better explain the severity of SZ than the functional ones. DTI has possessed the most stable results showing that bilateral medial lemniscus, and internal capsule are the most predictive biomarkers. They have great impacts on predicting the all types of PANSS score, which means they are related to a variety of syndromes in SZ. We can also find that fornix and UF, 2 important ROIs taking charge of working memory, are more related to the negative and general syndromes in SZ. For sMRI, limbic system is prevailing in score prediction. Especially for periarcheocortex [67], consisting of a complete anatomy system of cingulate gyrus, subcallosal area and PHG.

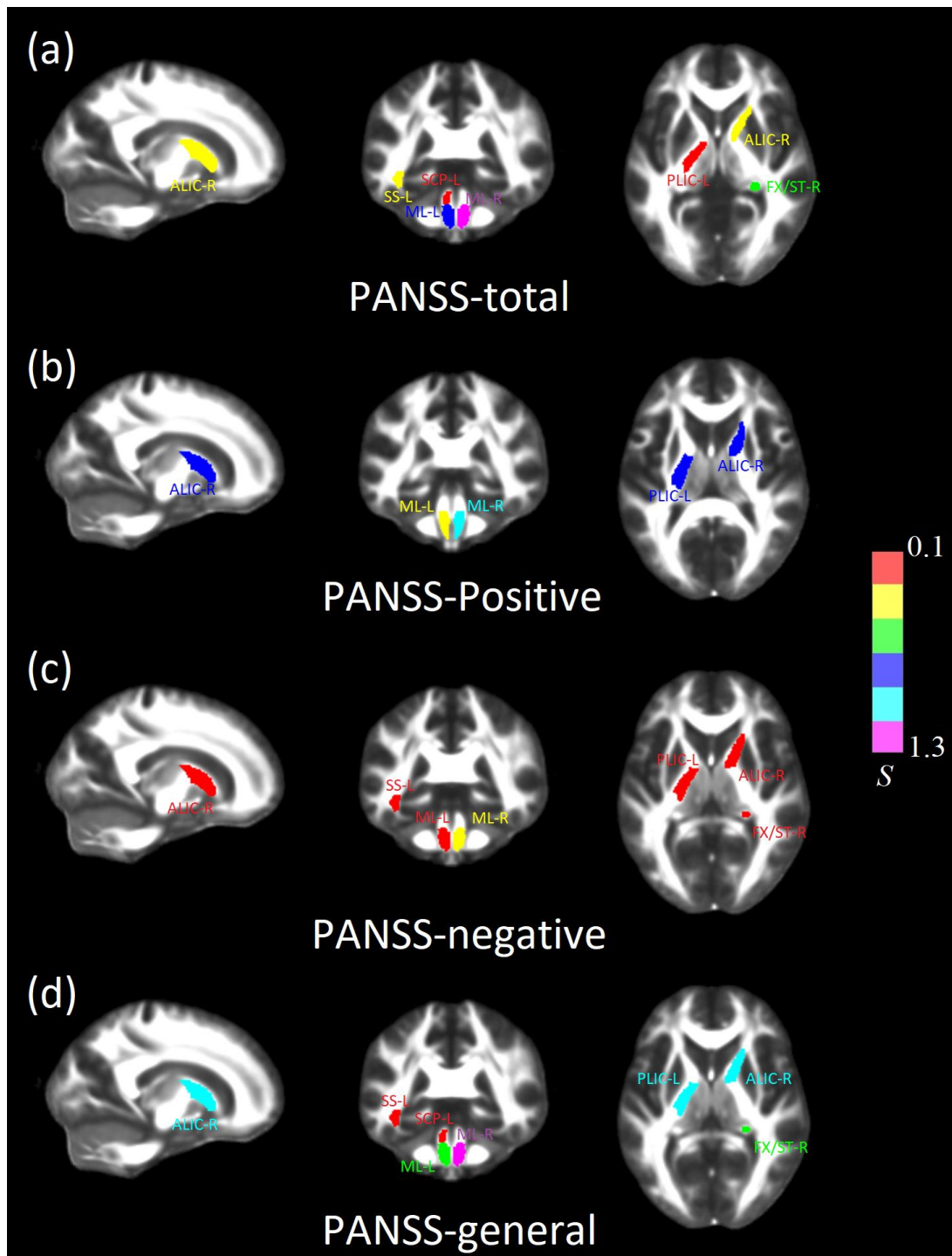
There have been 3 new findings worth reporting: 1) precentral gyrus (PCG), belonging to motor system, is among the all-round PANSS-score predictors. It suggests that motor retardation or out-of-control actions are not severe in first-episode patients but become severe when the disease goes on. 2) Abnormalities in frontal lobe have been

more frequently reported. Superior frontal sulcus (SFS) is most related to the general scores, and orbital sulcus and gyrus are found to be related to both positive and negative scores, which have been proved to be correlated with clinical scores among FES, chronic SZ, and schizoaffective disorder [68, 69]. Structural changes in frontal lobe are not sensitive in detecting FES, but they are useful in predicting specific syndrome scores. 3) Biomarkers of fALFF voxels in frontal lobe have also increased. Only the negative score seems to have small relation to the fALFF changes in brain. We conclude that limbic system, DMN, motor system, orbital/frontal lobe, and cerebellar connection will change according to the severity of SZ.



*The ROIs are mapped to the left hemisphere of surface. The color refers to the total value of S in the bilateral ROIs.

FIGURE 4.2 The important ROIs in sMRI measures in the surface map



*The values of S are divided into 6 levels globally.

FIGURE 4.3 The important ROIs in DTI measures

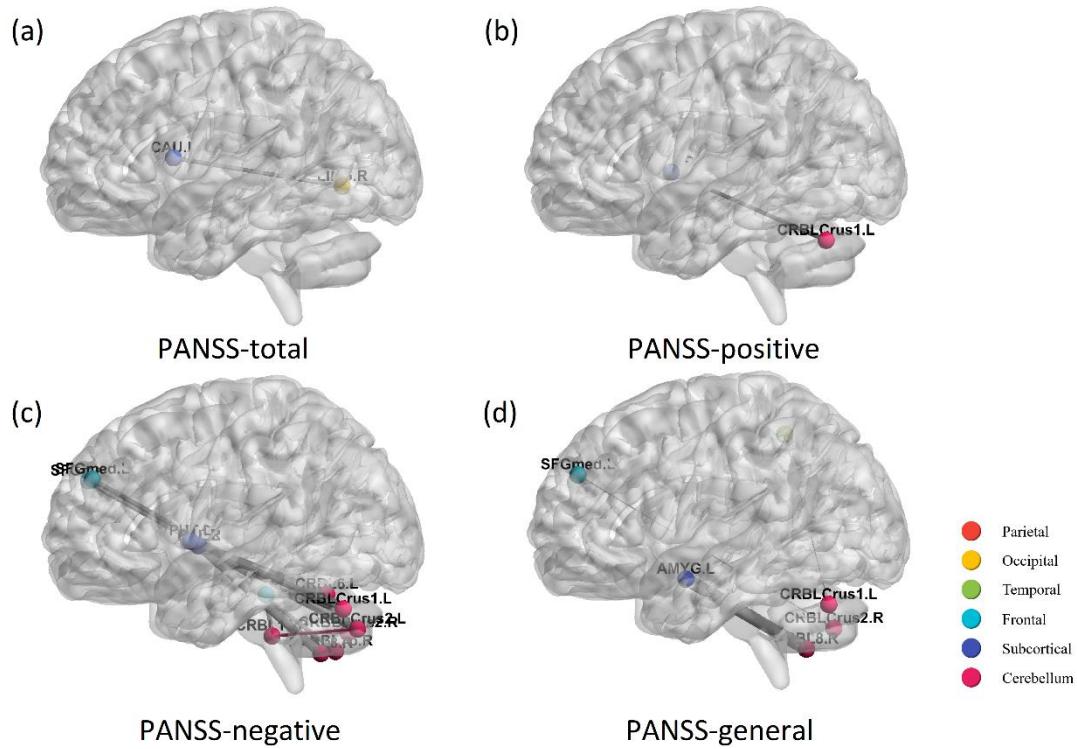


FIGURE 4.4 The topology graphs of selected FCs

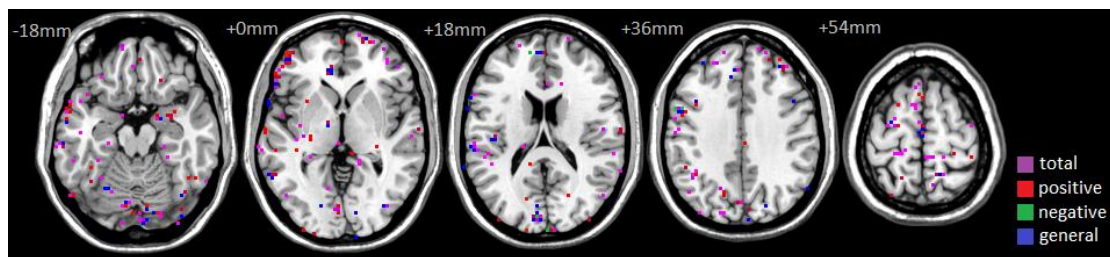


FIGURE 4.5 Map of selected voxels of fALFF in several axial slices

4.5 Chapter Summary

In this chapter, a multimodal regression model has been proposed for the multimodal analysis on the correlation of brain changes with clinical scores of SZ. The proposed method is a cogent regression model with double feature selection, has proved to achieve outstanding performance on both clinical score prediction and biomarker identification. Considering the data captured from different centers, the model has been realized in selecting appropriate groups of predictive features with validity and generality. This indicates the potential of our proposed model in identification of schizophrenic general pathology and auto-detection of disease level variation.

Chapter 5 Conclusion

In this study, we have developed the multimodal MR image analysis algorithms based machine learning methods for both classification and regression of SZ diagnosis. Based on 4 types of features extracted from 3 modalities of MR images, we have proposed a scheme of SC+SVM for the multimodal classification of first-episode schizophrenia patients and the healthy people; we have proposed a SC+RF combination method for multimodal regression to estimate the PANSS clinical scores and to find out predictive biomarkers for schizophrenia diagnosis. Both SC+SVM and SC+RF models have shown the effective multimodal combination, as well as the good feature selection, indicating that the achievements of machine learning based neuroimage analysis in auto-detection and diagnosis of psychosis.

For future work, we plan to focus on the longitudinal study of SZ. Based on our regression model, we aim to find the relationship between brain changes and other clinical factors, such as medical treatment, the course of disease. For this work, more longitudinal MR data are required to be collected. So, we may first make effort to recruit more participants. Or we can turn to some online databases including Schizconnect to choose conforming data. Furthermore, I am interested in applying machine learning to the stage of data acquisition. The ideal outcome is that more feature modalities can be extracted in spite of the tasks.

REFERENCE

- [1] Mitchell, [Machine Learning] McGraw-Hill, (2003).
- [2] W. H. Organization, "The World Health Report: mental disorders affect one in four people," (2001).
- [3] D. L. Segal, [Diagnostic and Statistical Manual of Mental Disorders (DSM - IV - TR)] American Psychiatric Association, (2000).
- [4] S. R. Kay, L. A. Opler, and J. P. Lindenmayer, "The Positive and Negative Syndrome Scale (PANSS): Rationale and standardisation," *British Journal of Psychiatry Supplement*(7), 59 (1989).
- [5] S. Teipel, A. Drzezga, M. J. Grothe *et al.*, "Multimodal imaging in Alzheimer's disease: validity and usefulness for early detection," *Lancet Neurology*, 14(10), 1037-1053 (2015).
- [6] T. K. Rajji, D. Miranda, and B. H. Mulsant, "Cognition, Function, and Disability in Patients With Schizophrenia: A Review of Longitudinal Studies," *Canadian Journal of Psychiatry Revue Canadienne De Psychiatrie*, 59(1), 13 (2014).
- [7] E. Rizos, M. A. Papathanasiou, P. G. Michalopoulou *et al.*, "A longitudinal study of alterations of hippocampal volumes and serum BDNF levels in association to atypical antipsychotics in a sample of first-episode patients with schizophrenia," *PLoS One*, 9(2), e87997 (2014).
- [8] J. Veijola, J. Y. Guo, J. S. Moilanen *et al.*, "Longitudinal changes in total brain volume in schizophrenia: relation to symptom severity, cognition and antipsychotic medication," *PLoS One*, 9(7), e101689 (2014).
- [9] C. C. Abbott, A. Jaramillo, C. E. Wilcox *et al.*, "Antipsychotic drug effects in schizophrenia: a review of longitudinal fMRI investigations and neural interpretations," *Current Medicinal Chemistry*, 20(3), 428-37 (2013).
- [10] P. Fusar-Poli, R. Smieskova, M. J. Kempton *et al.*, "Progressive brain changes in schizophrenia related to antipsychotic treatment? A meta-analysis of longitudinal MRI studies ☆," *Neuroscience & Biobehavioral Reviews*, 37(8), 1680 (2013).
- [11] B. C. Ho, "Long-term Antipsychotic Treatment and Brain Volumes," *Archives of General Psychiatry*, 68(2), 128 (2011).
- [12] K. R. Gray, P. Aljabar, R. A. Heckemann *et al.*, "Random forest-based similarity measures for multi-modal classification of Alzheimer's disease," *Neuroimage*, 65, 167-75 (2013).
- [13] G. Xu, and S. Huang, "Runway Incursion Event Forecast Model Based on LS-SVR with Multi-kernel," *Journal of Computers*, 6(7), 1346-1352 (2011).
- [14] N. Memarian, S. Kim, S. Dewar *et al.*, "Multimodal data and machine learning for surgery outcome prediction in complicated cases of mesial temporal lobe epilepsy," *Computers in Biology & Medicine*, 64, 67-78 (2015).
- [15] Y. M. Guo, P. He, X. T. Wang *et al.*, "Fast Prediction with Sparse Multikernel LS-SVR Using Multiple Relevant Time Series and Its Application in Avionics System," *Mathematical Problems in Engineering*, 2015,(2015-5-18), 2015(10), 1-10 (2015).
- [16] X. Gao, L. Fan, and H. Xu, "Multiple rank multi-linear kernel support vector machine for matrix data classification," *International Journal of Machine Learning & Cybernetics*, 1-11 (2015).
- [17] F. Liu, C. Y. Wee, H. Chen *et al.*, "Inter-modality relationship constrained multi-modality multi-

- task feature selection for Alzheimer's Disease and mild cognitive impairment identification," *Neuroimage*, 84, 466 (2014).
- [18] C. Zu, B. Jie, M. Liu *et al.*, "Label-aligned Multi-task Feature Learning for Multimodal Classification of Alzheimer's Disease and Mild Cognitive Impairment," *Brain Imaging & Behavior*, 10(4), 1148-1159 (2015).
- [19] X. Lele, W. Xia, C. Kewei *et al.*, "Multi-modality sparse representation-based classification for Alzheimer's disease and mild cognitive impairment," *Computer Methods & Programs in Biomedicine*, 122(2), 182-90 (2015).
- [20] G. Deanna, J. D. Malley, W. Brian *et al.*, "Using Multivariate Machine Learning Methods and Structural MRI to Classify Childhood Onset Schizophrenia and Healthy Controls," *Front Psychiatry*, 3, 53 (2012).
- [21] M. S. Çetin, F. Christensen, C. C. Abbott *et al.*, "Thalamus and posterior temporal lobe show greater inter-network connectivity at rest and across sensory paradigms in schizophrenia," *Neuroimage*, 97(2), 117 (2014).
- [22] C. J. Aine, H. J. Bockholt, J. R. Bustillo *et al.*, "Multimodal Neuroimaging in Schizophrenia: Description and Dissemination," *Neuroinformatics*, 15(4), 343-364 (2017).
- [23] J. R. Bustillo, T. Jones, H. Chen *et al.*, "Glutamatergic and Neuronal Dysfunction in Gray and White Matter: A Spectroscopic Imaging Study in a Large Schizophrenia Sample," *Schizophr Bull*, 43(3), 611 (2016).
- [24] F. B. S. DH, v. d. K. AJ *et al.*, "Sequence-independent segmentation of magnetic resonance images," *Neuroimage*, 23 Suppl 1(Suppl 1), S69 (2004).
- [25] M. Reuter, and B. Fischl, "Avoiding asymmetry-induced bias in longitudinal image processing," *Neuroimage*, 57(1), 19-21 (2011).
- [26] E. M. Sweeney, J. T. Vogelstein, J. L. Cuzzocreo *et al.*, "A comparison of supervised machine learning algorithms and feature vectors for MS lesion segmentation using multimodal structural MRI," *PLoS One*, 9(4), e95753 (2014).
- [27] S. M. Smith, M. Jenkinson, M. W. Woolrich *et al.*, "Advances in functional and structural MR image analysis and implementation as FSL," *Neuroimage*, 23(Suppl 1), S208-S219 (2004).
- [28] S. Raschka, "About Feature Scaling and Normalization and the effect of standardization for machine learning algorithms," *Polar Political & Legal Anthropology Review*, 30(1), 67-89 (2014).
- [29] Z. Lai, Z. Jin, and J. Yang, "Global Sparse Representation Projections for Feature Extraction and Classification." 1-5.
- [30] C. Lan, X. Y. Jing, S. Li *et al.*, "Exploring the natural discriminative information of sparse representation for feature extraction." 916-920.
- [31] J. Wright, A. Ganesh, Z. Zhou *et al.*, "Demo: Robust face recognition via sparse representation." 1-2.
- [32] J. Lai, and X. Jiang, "Class-wise Sparse and Collaborative Patch Representation for Face Recognition," *IEEE Trans Image Process*, 25(7), 3261-3272 (2016).
- [33] D. Ghosh, and A. M. Chinnaiyan, "Classification and selection of biomarkers in genomic data using LASSO," *Journal of Biomedicine & Biotechnology*, 2005(2), 147 (2005).
- [34] R. Tibshirani, "Regression Shrinkage and Selection via the Lasso," *Journal of the Royal Statistical Society: Series B (Statistical Methodology)*, 73(3), 267-288 (2011).

- [35] M. Liu, D. Zhang, and D. Shen, "Identifying informative imaging biomarkers via tree structured sparse learning for AD diagnosis," *Neuroinformatics*, 12(3), 381-394 (2014).
- [36] C. C. Chang, and C. J. Lin, "LIBSVM: A library for support vector machines," *Acm Transactions on Intelligent Systems & Technology*, 2(3), 1-27 (2011).
- [37] C. Destrieux, B. Fischl, A. Dale *et al.*, "Automatic parcellation of human cortical gyri and sulci using standard anatomical nomenclature," *Neuroimage*, 53(1), 1-15 (2010).
- [38] S. D. Santis, Y. Assaf, and D. K. Jones, "Using the biophysical CHARMED model to elucidate the underpinnings of contrast in diffusional kurtosis analysis of diffusion-weighted MRI," *Magnetic Resonance Materials in Physics Biology & Medicine*, 25(4), 267-276 (2012).
- [39] F. Liu, W. Guo, J. P. Fouche *et al.*, "Multivariate classification of social anxiety disorder using whole brain functional connectivity," *Brain Structure & Function*, 220(1), 101-115 (2015).
- [40] N. C. Andreasen, and R. Pierson, "The Role of the Cerebellum in Schizophrenia," *Biological Psychiatry*, 64(2), 81-8 (2008).
- [41] G. Collin, H. E. H. Pol, S. V. Haijma *et al.*, "Impaired Cerebellar Functional Connectivity in Schizophrenia Patients and Their Healthy Siblings," *Front Psychiatry*, 2(73), 73 (2011).
- [42] T. Kasparek, J. Rehulova, M. Kerkovsky *et al.*, "Cortico-cerebellar functional connectivity and sequencing of movements in schizophrenia," *BMC Psychiatry*, 12, 1(2012-03-12), 12(1), 17 (2012).
- [43] W. Guo, F. Zhang, F. Liu *et al.*, "Cerebellar abnormalities in first-episode, drug-naive schizophrenia at rest," *Psychiatry Research*, (2018).
- [44] J. D. Schmahmann, "The cerebrocerebellar system: anatomic substrates of the cerebellar contribution to cognition and emotion," *International Review of Psychiatry*, 13(4), 247-260 (2001).
- [45] W. Guo, F. Liu, J. Chen *et al.*, "Hyperactivity of the default-mode network in first-episode, drug-naive schizophrenia at rest revealed by family-based case-control and traditional case-control designs," *Medicine*, 96(13), e6223 (2017).
- [46] W. Guo, D. Yao, J. Jiang *et al.*, "Abnormal default-mode network homogeneity in first-episode, drug-naive schizophrenia at rest," *Prog Neuropsychopharmacol Biol Psychiatry*, 49(2), 16-20 (2014).
- [47] Z. He, W. Deng, M. Li *et al.*, "Aberrant intrinsic brain activity and cognitive deficit in first-episode treatment-naive patients with schizophrenia," *Psychological Medicine*, 43(4), 769-80 (2013).
- [48] H. Wang, W. Guo, L. Feng *et al.*, "Patients with first-episode, drug-naive schizophrenia and subjects at ultra-high risk of psychosis shared increased cerebellar-default mode network connectivity at rest," *Sci Rep*, 6, 26124 (2016).
- [49] J. R. Andrews - Hanna, J. Smallwood, and R. N. Spreng, "The default network and self-generated thought: component processes, dynamic control, and clinical relevance," *Annals of the New York Academy of Sciences*, 1316(1), 29 (2014).
- [50] J. Chen, D. Wei, L. Yang *et al.*, "Neurocognitive impairment on motor imagery associated with positive symptoms in patients with first-episode schizophrenia: evidence from event-related brain potentials," *Psychiatry Res*, 231(3), 236-243 (2015).
- [51] K. P. Wylie, and J. R. Tregellas, "The role of the insula in schizophrenia," *Schizophr Res*, 123(2-3), 93-104 (2010).

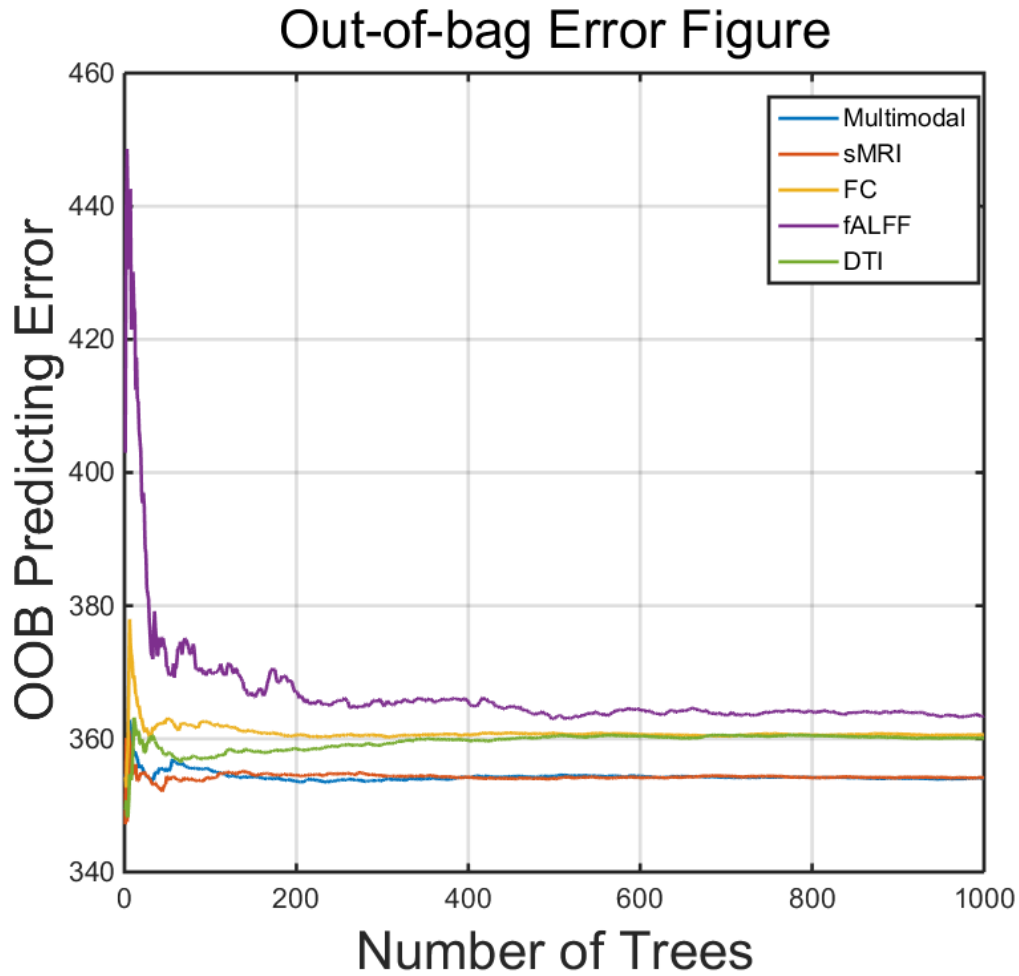
- [52] S. Marengo, J. L. Stein, A. A. Savostyanova *et al.*, "Investigation of Anatomical Thalamo-Cortical Connectivity and fMRI Activation in Schizophrenia," *Neuropsychopharmacology Official Publication of the American College of Neuropsychopharmacology*, 37(2), 499 (2012).
- [53] S. S. Bolkan, J. M. Stujenske, S. Parnaudeau *et al.*, "Thalamic projections sustain prefrontal activity during working memory maintenance," *Nature Neuroscience*, 20(7), (2017).
- [54] H. T. Ito, S. J. Zhang, M. P. Witter *et al.*, "A prefrontal-thalamo-hippocampal circuit for goal-directed spatial navigation," *Nature*, 522(7554), 50 (2015).
- [55] P. A. Domen, S. Michielse, E. Gronenschild *et al.*, "Microstructural white matter alterations in psychotic disorder: a family-based diffusion tensor imaging study," *Schizophrenia Research*, 146(1-3), 291 (2013).
- [56] A. Caprihan, T. Jones, H. Chen *et al.*, "The Paradoxical Relationship Between White Matter, Psychopathology and Cognition in Schizophrenia: A Diffusion Tensor and Proton Spectroscopic Imaging Study," *Neuropsychopharmacology*, 40(9), 2248 (2015).
- [57] J. Fitzsimmons, M. Kubicki, K. Smith *et al.*, "Diffusion tractography of the fornix in schizophrenia," *Schizophrenia Research*, 107(1), 39-46 (2009).
- [58] Y. Zhou, N. Shu, Y. Liu *et al.*, "Altered resting-state functional connectivity and anatomical connectivity of hippocampus in schizophrenia," *Schizophrenia Research*, 100(1), 120-132 (2008).
- [59] S. Poletti, E. Mazza, I. Bollettini *et al.*, "Adverse childhood experiences influence white matter microstructure in patients with schizophrenia," *Psychiatry Res*, 234(1), 35-43 (2015).
- [60] M. D. Bell, P. H. Lysaker, R. M. Milstein *et al.*, "Concurrent validity of the cognitive component of schizophrenia: relationship of PANSS scores to neuropsychological assessments," *Psychiatry Research*, 54(1), 51-58 (1994).
- [61] L. Breiman, "Bagging predictors," *Machine Learning*, 24(2), 123-140 (1996).
- [62] M. R. Segal, "Machine Learning Benchmarks and Random Forest Regression," *Center for Bioinformatics & Molecular Biostatistics*, (2004).
- [63] V. Svetnik, A. Liaw, C. Tong *et al.*, "Random forest: a classification and regression tool for compound classification and QSAR modeling," *Journal of Chemical Information & Computer Sciences*, 43(6), 1947 (2003).
- [64] C. Englund, J. Kovaceva, M. Lindman *et al.*, "Using Random Forests for Data Mining and Drowsy Driver Classification Using FOT Data." 752-762.
- [65] J. Seoane, I. Day, C. Campbell *et al.*, "Using a Random Forest proximity measure for variable importance stratification in genotypic data," (2014).
- [66] M. A. A. Cox, and T. F. Cox, "Multidimensional Scaling," *Journal of the Royal Statistical Society*, 46(2), 1050-1057 (2001).
- [67] J. F. Schneider, and K. Vergesslich, "Maturation of the limbic system revealed by MR FLAIR imaging," *Pediatric Radiology*, 37(4), 351-355 (2007).
- [68] M. J. Hoptman, J. Volavka, E. M. Weiss *et al.*, "Quantitative MRI measures of orbitofrontal cortex in patients with chronic schizophrenia or schizoaffective disorder," *Psychiatry Research Neuroimaging*, 140(2), 133-45 (2005).
- [69] A. L. Lacerda, A. Y. Hardan, O. Yorbik *et al.*, "Morphology of the orbitofrontal cortex in first-episode schizophrenia: relationship with negative symptomatology," *Prog Neuropsychopharmacol Biol Psychiatry*, 31(2), 510-6 (2007).

APPENDIX

Appendix I The identified sMRI and DTI biomarkers by SR in classification

	Brain Region	Feature	Hemisphere
sMRI			
No.49	Superior segment of the circular sulcus of the insula	Thickness	Left
No.36	Planum temporale or temporal plane of the superior temporal gyrus	Mean curvature	Left
No.51	Posterior transverse collateral sulcus	Curvature index	Left
No.17	Long insular gyrus and central sulcus of the insula	Curvature index	Right
DTI			
No.26	Superior corona radiate	FA	Left
No.40	Fornix / terminal stria	FA	Left
No.37	Cingulum (hippocampus)	FA, MD	Right
No.47	Uncinate fasciculus	MD	Right
No.30	Posterior thalamic radiation (include optic radiation)	FA	Left
No.29	Posterior thalamic radiation (include optic radiation)	MD	Right
No.13	Superior cerebellar peduncle	MD	Right
No.35	Cingulum (cingulate gyrus)	MD	Right

Appendix II Out-of-bag error figure



Appendix III The predictive biomarkers of sMRI and DTI in SR+RF regression

sMRI

(a) PANSS-total score

ROI No.	Label name	Importance
43	Pole_temporal	0.4074
59	S_occipital_ant	0.3990
69	S_precentral-sup-part	0.3923
9	G_cingul-Post-dorsal	0.3172
66	S_pericallosal	0.2946
23	G_oc-temp_med-Parahip	0.2381
18	G_insular_short	0.2264
29	G_precentral	0.2168
65	S_parieto_occipital	0.2092
45	S_central	0.1622
10	G_cingul-Post-ventral	0.1583
32	G_subcallosal	0.1392
48	S_circular_insula_inf	0.1109
22	G_oc-temp_med-Lingual	0.1045
68	S_precentral-inf-part	0.0999

(b) PANSS-positive score

ROI No.	Label name	Importance
66	S_pericallosal	0.6551
59	S_occipital_ant	0.4482
69	S_precentral-sup-part	0.4311
32	G_subcallosal	0.4233
48	S_circular_insula_inf	0.3879
54	S_front_sup	0.3820
51	S_collat_transv_post	0.3755
43	Pole_temporal	0.3222
64	S_orbital-H_Shaped	0.2772
45	S_central	0.2628
10	G_cingul-Post-ventral	0.2091
68	S_precentral-inf-part	0.2028
30	G_precuneus	0.1658
23	G_oc-temp_med-Parahip	0.1427
9	G_cingul-Post-dorsal	0.1198
18	G_insular_short	0.1140

(c) PANSS-negative score

ROI No.	Label name	Weight
69	S_precentral-sup-part	0.5415
30	G_precuneus	0.5264
66	S_pericallosal	0.4960
8	G&S_cingul-Mid-Post	0.3978
58	S_oc_sup&transversal	0.3869
64	S_orbital-H_Shaped	0.3784
43	Pole_temporal	0.3770
68	S_precentral-inf-part	0.3419
9	G_cingul-Post-dorsal	0.2853
48	S_circular_insula_inf	0.2564
54	S_front_sup	0.2463
29	G_precentral	0.2453
18	G_insular_short	0.2265
59	S_occipital_ant	0.1985
6	G&S_cingul-Ant	0.1768
10	G_cingul-Post-ventral	0.1576
32	G_subcallosal	0.1460
17	G_Ins_lg&S_cent_ins	0.1040
7	G&S_cingul-Mid-Ant	0.1024

(d) PANSS-general score

ROI No.	Label name	Weight
43	Pole_temporal	0.5970
59	S_occipital_ant	0.4926
69	S_precentral-sup-part	0.4280
9	G_cingul-Post-dorsal	0.4246
66	S_pericallosal	0.3356
23	G_oc-temp_med-Parahip	0.3257
18	G_insular_short	0.2549
29	G_precentral	0.2517
65	S_parieto_occipital	0.2501
45	S_central	0.2245
10	G_cingul-Post-ventral	0.2221
32	G_subcallosal	0.1941
48	S_circular_insula_inf	0.1691
22	G_oc-temp_med-Lingual	0.1358
68	S_precentral-inf-part	0.1186

DTI

(a) PANSS-total score

ROI No.	label name	Measure	Importance
9	Medial lemniscus R	FA	1.1191
10	Medial lemniscus L	FA	0.8971
39	Fornix (cres) / Stria terminalis (can not be resolved with current resolution) R	FA	0.6378
32	Sagittal stratum (include inferior longitudinal fasciculus and inferior fronto-occipital fasciculus) L	MD	0.3657
17	Anterior limb of internal capsule R	FA	0.2936
14	Superior cerebellar peduncle L	FA	0.2276
20	Posterior limb of internal capsule L	MD	0.1882

(b) PANSS-positive score

ROI No.	label name	Measure	Importance
9	Medial lemniscus R	FA	1.0120
17	Anterior limb of internal capsule R	FA	0.8807
20	Posterior limb of internal capsule L	MD	0.7173
10	Medial lemniscus L	FA	0.3798

(c) PANSS-negative score

ROI No.	label name	Measure	Importance
9	Medial lemniscus R	FA	0.3327
20	Posterior limb of internal capsule L	MD	0.2132
10	Medial lemniscus L	FA	0.1619
17	Anterior limb of internal capsule R	FA	0.1314
39	Fornix (cres) / Stria terminalis (can not be resolved with current resolution) R	FA	0.0918
32	Sagittal stratum (include inferior longitudinal fasciculus and inferior fronto-occipital fasciculus) L	MD	0.0848

(d) PANSS-general score

ROI No.	label name	Measure	Importance
9	Medial lemniscus R	FA	1.3112
20	Posterior limb of internal capsule L	MD	1.0127
17	Anterior limb of internal capsule R	FA	0.9877
39	Fornix (cres) / Stria terminalis (can not be resolved with current resolution) R	FA	0.6863

(d) PANSS-general score

ROI No.	label name	Measure	Importance
10	Medial lemniscus L	FA	0.5062
32	Sagittal stratum (include inferior longitudinal fasciculus and inferior fronto-occipital fasciculus) L	MD	0.2528
14	Superior cerebellar peduncle L	FA	0.2334

ACKNOWLEDGEMENTS

This work is supported in part by NSFC grants (No. 61375112, 61773263), the National Key Research and Development Program of China (No.2016YFC0100903), and SMC Excellent Young Faculty program of SJTU. We appreciate SMHC for providing MR data, and Mrs. Xu Jiale for the clinical score collection. I feel grateful to the senior students Mrs. Meng Ziyu and Mrs. Wang Danni in Med-X Research Institute who offered great assistance to the result representation of fMRI and DTI. I also learned a lot about these two MR techniques from them. Thanks for the fellows in Lab 2-322. They have created an incredible environment of the lab and have provided me with meticulous help over the past year.

I'd love to present my sincere thanks to my research partners: Mr. Liu Ruihao, Mr. Wu Chaowei, and 3 former partners: Mr. Fang Yubo, Mr. Chen Xuelei, and Mr. He Hao, who have made great contribution to the research. I treasure the time with your guys striving for the better results. You are my friends, also act as my advisors. Thank you for your company.

I will next give my greatest appreciation to my advisors: Professor Liu Manhua and Professor Li Yao. Though I am not a student of Professor Li, she still put great force to teach me the knowledge of brain and MR techniques. She also spent a lot of time in revising the paper for me. She offered me many chances for MR data processing and more access to the frontier technology of neuroscience. Dear Professor Liu, a great advisor purely devotes herself to the researches, gives me a lot of opportunities despite my shallow knowledge. She is pretty enlightened to accept any potential proposals raised by me and spare no effort in supporting me to accomplish them. She also gave me considerable suggestions, criticism, and concerns. She gave me almost any possible tasks of projects, though I am just an undergraduate student, which I believe almost no one had such adequate opportunities. I've learned a lot from Professor Liu, and she takes me into another level.

I am greatly indebted to Professor Liu Hua, my first advisor who awake me from ignorance. I also appreciate Professor Xiong Liqin and Professor Zhao Jun, who teach me molecular imaging and medical imaging processing. All of them raised my interest in this field and helped me establish the cogent basis of knowledge. Many thanks to the classmates and teachers in our department, and my lovely roommates who provide me with a happy environment for study. Last but not least, Miss Wu Yina, thank you for giving me hope and happiness when I felt weary. I'll always remember this period of time.

PUBLICATIONS

1. Huixiang Zhuang, Yao Li, Ruihao Liu, Chaowei Wu and Manhua Liu*, “Multimodal Analysis of Structural and Functional MRI for Schizophrenia Diagnosis” Proceedings of 9th International Conference on Digital Image Processing (ICDIP) 2018, Shanghai, China, May 11-14.
2. Zhuang H., Liu M., Liu R., etc. “Multimodal classification of drug-naïve first-episode schizophrenia combining anatomical, diffusion and resting state functional resonance imaging”, Submitted to 《Neuroimage: clinical》